Archives of Materials Science and Engineering

Volume 123
Issue 1
September 2023
Pages 13-29

International Scientific Journal
published monthly by the
World Academy of Materials
and Manufacturing Engineering

DOI: 10.5604/01.3001.0053.9754

An experimental and theoretical piezoelectric energy harvesting from a simply supported beam with moving mass

A.M. Mohaisen *, T.J. Ntayeesh
Mechanical Engineering Department, University of Baghdad, Baghdad, Iraq
* Corresponding e-mail address: a.chaabari1803m@coeng.uobaghdad.edu.iq
ORCID identifier: https://orcid.org/0000-0001-8624-9787 (T.J.N.)

ABSTRACT

Purpose: The feasibility of harvesting electrical energy from mechanical vibration is demonstrated in the thesis. In the technique, energy is harvested from simply supported beam vibration under a moving mass using a thin piezoelectric material.

Design/methodology/approach: The structure is represented by a basic beam of length L that is supported at both ends and traversed by a moving mass M travelling at a constant velocity v. The Euler-Bernoulli differential equation describes its behaviour. The dynamic analysis of a beam is performed by using three moving masses of (35.61, 65.81, and 79.41) gr each travelling three uniform speeds of (1.6, 2 and 2.4) m/s. A differential equation of the electromechanical system is obtained by transforming the piezoelectric constitutive equation and solved numerically by MATLAB.

Findings: The results indicate that the numerical and experimental values for the midpoint deflection of the beam and the piezoelectric voltage are very close.

Research limitations/implications: Using the COMSOL programme, the proposed approach is checked by comparing results with data obtained by the finite element method (FEM). An experimental setup was also built and constructed to determine the voltage created by the piezoelectric patch and the beam response as a result of the mass travelling along the beam.

Practical implications: The results show that the dynamic deflection, piezoelectric voltage, and piezoelectric energy harvesting all increase as the speed and magnitude of the moving mass increase. The harvesting power vs. load resistance curve begins at zero, increases to a maximum value, and then remains almost constant as the resistance is increased further. The optimal length of the piezoelectric patch was obtained to be 0.63 m. When the length of the beam increases, the resonant frequency decreases, and at the same time the harvested energy increases. However, increasing the beam thickness has the opposite effect; whereas raising the beam width does not affect the resonant frequency but decreases energy harvesting.

Originality/value: The most essential point here is the need to have correctly built scale models. They can provide a substantial amount of information at a low cost, accommodate a variety of test settings, and aid in the selection and verification of the most effective analytical model to resolve the actual issue.

Keywords: Time response, Moving mass, Electrical energy, Energy harvesting, Bridge vibration, Piezoelectric

Reference to this paper should be given in the following way:
A.M. Mohaisen, T.J. Ntayeesh, An experimental and theoretical piezoelectric energy harvesting from a simply supported beam with moving mass, Archives of Materials Science and Engineering 123/1 (2023) 13-29. DOI: https://doi.org/10.5604/01.3001.0053.9754

1. Introduction

Energy harvesting has garnered considerable attention from a variety of disciplines in recent years, owing to its potential significance as a critical technology for electronic systems that are self-powered and consume very little electricity. Energy harvesting, in general, is the process of extracting ambient energy from the environment that surrounds a system and converting it into another form (often electricity) and then using that energy to provide energy for the system described above. It is in contrast to powering a system with sources of energy that are finite, like oil, batteries, coal, or fuel cells [1]. Piezoelectric materials are frequently employed as transducers, converting electrical energy to force or mechanical motion, as well as in the opposite direction. Due to piezoelectric materials' ability to convert mechanical power into electrical power, ambient motion (typically vibration) can be converted to electrical energy stored and used by electronic devices like sensor transmitters. Analysis modelling is a critical component of a design phase for learning the interactions between different parameters and optimising critical design parameters throughout the implementation and analysis of these energy harvesting systems [2]. To understand the response of beams to moving loads or moving masses, several studies have been conducted in the past.The following paragraphs summarise their works. M.A. Foda and Z. Abduljabbar 1997 [3] used a dynamic Green function approach to determine the response of a supported Bernoulli Euler beam of finite length subject to a moving mass traversing its span. The proposed method yields a straightforward matrix formula for the beam's deflection. Numerous numerical examples demonstrate the method's efficiency and simplicity. L. Fryba 1999 [4] summarised the dynamic impacts of railway bridges. Emphasis was placed on traffic loads and their effect on railway bridge reaction. The fundamental dynamic properties of railway bridges are detailed, as well as the effect of the most critical parameters, like track imperfections and vehicle speed. Aside from vertical impacts, the transverse effects and horizontal longitudinal on bridges were also considered. Wind and seismic effects, on the other hand, are ignored. The goal of this paper was to provide a thorough examination of the dynamic behaviour of railway bridges, to give an abundance of experimental results, and to illustrate effectively applied methods for dynamic problems. C. Bilello et al. 2004 [5] studied the dynamic response of a small-scale bridge model under a moving mass. The study is based on the continuous Euler-Bernoulli beam theory. The provided problem is simplified to the solution of a set of linear differential equations of second order involving time-varying coefficients by expanding the unknown structural response in a series of the beam Eigen functions. Through a series of trials, the analytical solution is validated. The measured response was marginally larger than that predicted analytically, and in the speed range examined, there was no discernible difference between moving mass and moving force solutions. S.H. Bakhy et al. 2021 [6] studied the free vibration analysis of sandwich beams made of functionally graded materials (FGMs) with various core metals and wall thicknesses. Based on the Euler-Bernoulli beam theory, a mathematical formulation has been developed for a sandwich beam that consists of an FG core sandwiched between two layers of ceramic and metal, with homogeneous material making up the face sheets. It became clear that the ratio, index of volume fraction, and face FGM core ingredients all significantly impacted the dynamic response, the mode forms, and the natural frequency characteristics. E. Abdeddine et al 2022 [7] proposed an experimental investigation into how a cantilever and a rectangular plate manufactured using the fused filament fabrication process are affected by large vibration. By stimulating the plate at a large displacement, the structure's nonlinear dynamic behaviour during forced vibration is calculated. For the first, second, and third mode shapes., the relationship between frequency and amplitude vibration is investigated. The research of piezoelectric energy harvesting technology has grown in prominence. The research of piezoelectric energy harvesting technology has grown in prominence. The following paragraphs summarise some previous studies about it. S. F. Ali et al. 2011 [8] examined the potential for piezoelectric energy harvesters to be used as scavenging devices for energy on highway bridges. The model of a motorway bridge with a shifting point load is explored, and the piezoelectric energy harvester is modelled using a model with a single degree of freedom. Two distinct

types of harvesters have been investigated, specifically, the circuit for harvesting with and without an inductor. The energy generated by a single vehicle has been evaluated. Those results, combined with traffic information, can be utilised to determine the variance in average power and thus aid in the design system of energy management for a particular application. A. Erturk and D.J. Inman 2011 [9] proposed two methodologies for piezoelectric energy production from dynamic loading. The first is predicated on using a cantilevered bimorph positioned arbitrarily on a thin bridge that is supported. The second method contemplates using a thin patch of piezoceramic to cover a section of the bridge. Y. Zhang and L. Deng 2014 [10] discussed piezoelectric energy harvesting from civil infrastructures. Due to their widespread use, piezoelectric cantilever-based harvesters are adopted. Simulated has been done for bridge-vehicle systems in two different scenarios: with a single passing vehicle and with a continual flow of vehicles. Parametric research is done to determine the influence of various numerous vehicles and bridges on energy harvesting. The simulation outcome indicates that the power of energy output rises when road conditions deteriorate and lengths of bridge spans decrease. Additionally, this article investigates and discusses optimum vehicle speeds and energy harvester placements. S. Senthil Murugan, P. Vijayakumar 2017 [11] studied the exploration of ultrasonic frequency for producing water mist without a pressurised system. Using a piezoelectric transducer, the H-bridge circuit has been constructed. It will function between 0 and 3 MHz. The minimum frequency needed to generate water mist is approximately 2 MHz, which has been predicted using the established model. The results of the experiments have shown that water mist generation in the water reservoir requires a minimum of 2 MHz .K. Bendine et al. 2019 [12] studied a finite element model of the bridge (cantilever beam) for time domain analysis using Hamilton principle, the Kirchhoff plate assumptions, and the Newmark integration scheme. Considerations are made for various sorts of moving loads (broadband, narrow-band, constant and harmonic). The acquired results reflect prior findings in the literature: when the harvester is situated at the highest amplitude of the bridge's associated mode shape, the gathered energy is maximal. These findings are not confirmed when genuine moving loads are used in conjunction with a narrow-banded or broadband frequency spectrum. Z. Yang et al. 2020 [13] employed the perturbation of biparameters approach to address the free vibration damping issue for cantilever beams with piezoelectric, and the solution of the perturbation to the problem was presented. The effect of piezoelectric characteristics on piezoelectric cantilever beams vibrate was demonstrated numerically. Additionally, vibration studies on cantilever beams with piezoelectric, were conducted, and the practical results agreed well with the theoretical predictions. The results imply that the solution to the biparametric perturbation problem produced is effective in their study, and it may be used as a theoretical reference for designing piezoelectric actuators and sensors. J.X. Wang et al. 2022 [14] presented a multi-folded-beam piezoelectric energy harvester (MFB-PEH) for low-power energy harvesting applications in settings with low frequencies and low amplitude vibrations. In order to find the best design, the finite element technique (FEM) was first employed. According of the experimental findings, the improved MFB-PEH has three resonance frequencies in the 9 to 20 Hz range of the surrounding frequency, which can increase the harvester's operational bandwidth. To capture the energy produced by human motion, a bundled MFB-PEH was finally used. Our research has demonstrated the MFB-PEH's suitability as a potential generator in situations with low frequencies and amplitudes, as well as a wide frequency range. Xiong C et al. 2023 [15] introduced a low-cost, magnet-free, bistable piezoelectric energy harvester to capture energy from low-frequency vibration, transform it into electrical energy, and lessen fatigue damage brought on by stress concentration. The flapping wings of seagulls inspired it during flight. Finite element modelling was used to quantitatively examine the energy harvester's greater performance in reducing stress concentration compared to the prior parabolic one employing bistable technology, with a maximum stress reduction of 32.34%. According to the testing findings, the harvester's highest open-circuit voltage and maximum output power were 11.5 V and 73 W, under ideal working circumstances.

Much research has been conducted, but in the research, energy was harvested using three moving masses with three speeds for each of those masses, as well as studying the state of the beam when the moving mass exits. It also compares the results practically and numerically using MATLAB and COMSOL programs to get more accurate results. This research will construct trustworthy theoretical models that accurately predict output piezoelectric power values, hence avoiding the time-consuming procedure of fabricating a structure, testing setup and completing time-consuming measurements. Parametric research will also be undertaken to enhance the power collecting process; PZT length, resistive load and beam dimensions will be examined in order to identify how they affect the power output and to optimise the PZT's possible output power coupled to a supported beam.

2. Theoretical background

The Dynamic equilibrium equation will initially be displayed. Then a statement of how the mathematical equations will be simplified and solved.

2.1. Dynamic equilibrium equation

Consider a moving mass M move at speed v connected to a Euler-Bernoulli beam with length L, as shown in Figure 1. It is supposed that the beam and moving mass are linked and that the moving object's transverse vibration in relation to the beam is insignificant. When analysing a moving mass, it is necessary to consider its inertial effects. As a result, energy techniques should be used to determine the governing equation. Substituting x in y(x,t) with the value of x(t) would yield the displacements of the beam and the moving mass relative to the mass's position, expressed clearly in terms of time. The physical function that depicts the projections of mass-related displacements is denoted by [16].

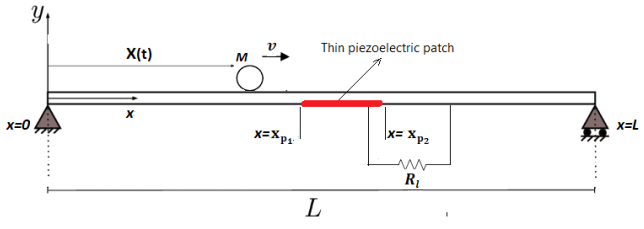

Fig. 1. Diagram of a beam with moving mass

$$Y(t) = y(X,t) \tag{1}$$

The system's potential and kinematical energy at time t are applied to use Hamilton's principle and derive the governing equation. As a result, the equation of dynamic equilibrium for a moving mass load is regarded as [9,16]:

$$EI\frac{\partial^4 y(x,t)}{\partial x^4} + c_s I\frac{\partial^5 y(x,t)}{\partial x^4\,\partial t} + c_a\frac{\partial y(x,t)}{\partial t} + m\frac{\partial^2 y(x,t)}{\partial t^2} = \delta(x - vt)P(x,t) \tag{2}$$

where the mass of beam $m = \rho A$, represented the bending stiffness, equivalent coefficient of strain rate damping, viscous air damping coefficient and dirac delta function respectively. Assuming that the mass has a vertical displacement $y(x,t)$, the applying force $P(x,t)$ on the beam could be written as [17]:

$$P(x,t) = Mg - M\frac{d^2 y(x,t)}{dt^2} \tag{3}$$

The following could be deduced from the assumption of no separation [17]:

$$P(x,t) = Mg - M\left(\frac{\partial^2 y(x,t)}{\partial t^2} + 2v\frac{\partial^2 y(x,t)}{\partial x\,\partial t} + v^2\frac{\partial^2 y(x,t)}{\partial x^2}\right) \tag{4}$$

In Eq.(4), Items in parentheses have the following physical significance: $\partial^2 y(x,t)/\partial t^2$ represents vertical acceleration caused by beam vibration; $2v\,\partial^2 y(x,t)/\partial x\partial t$ represents vertical acceleration caused by a change in the vertical speed of the beam caused by load movement; and $\partial^2 y(x,t)/\partial x^2$) represents centrifugal acceleration caused by load moving along the vertical curve caused by beam vibration [17,18].

It is important to notice that x is set exclusively for locations on beam, and hence $0 \le x \le$ L valid. It is accomplished using the delta function that appears on the right side of Eq. (2); it ensures that only the beam is affected by the weight that is moving across it. A proper set of initial and boundary conditions must be used in conjunction with Eq. (2). Because Eq. (2) is indeed a (PDE), a solution of the following form is assumed [16]:

$$y(x,t) = \sum_{r=1}^{\infty} \phi_r(x)\eta_r(t) \tag{5}$$

where ϕ_r(x) denotes the beam's rth mode shape function and the rth modal displacement of the beam, represented by the symbol η_r(t). There are unlimited modes for the exact beam solution, implying that the overall solution would require an endless series; this series is represented by Eq. (5), N-terms truncated. Where ϕ_r(x), the mode shapes are time-independent and fulfil the boundary conditions. Nonetheless, the modal displacements, η_r(t), are spatially independent and satisfy the PDE's initial conditions. For supported uniform beams, the mass normalised mode shapes are given by sine functions [19]; therefore,

$$\phi_r(x) = \sqrt{2/mL}\sin(r\pi x/L) \tag{6}$$

Which satisfies the orthogonality conditions:

$$\int_0^L \phi_s(x)m\phi_r(x)\mathrm{d}x = \delta_{rs}\ ,\int_0^L \phi_s(x)EI\frac{d^4\phi_r(x)}{dx^2}dx = \omega_r^2\delta_{rs} \tag{7}$$

where δ_{rs} is the Kronecker delta, defined as one for s = r and zero for $s \neq r$, and ω_r is the undamped natural frequency of the beam's rth mode [10]. There is also the exciting frequency ω [4].

$$\omega_r = \pi^2 r^2\sqrt{EI/mL^4} \tag{8.a}$$

$$\omega = \frac{r\pi\, v}{L} \tag{8.b}$$

The moving mass's critical velocity at which beam resonance [4]:

$$v_c = \frac{\pi}{L}\sqrt{EI/m} = \frac{L\,\omega_1}{\pi} \tag{9}$$

Eq. (2) is solved on the basis of the following assumptions [9]:

i) The assumptions underlying the structure are:
   a) Small structural deformations,
   b) Material with linear elastic properties,
   c) Initially straight beams,
ii) The effects of shear deformation as well as rotating inertia, are ignored (Euler-Bernoulli beam). As a result, the beam has a small height-to-length ratio.
iii) The mass goes from left to right at a constant speed.

2.2. Differential equation of motion discretisation

In order to simplify the analyses of motion differential equations, the dimensionless high order differential equation (2) is discretised and decreased order to a lower order differential equation via Ritz-Galerkin method [17]. Supposing displacement y as a function of variables x and t, and its Ritz-Galerkin expression will be as in Eq. (5) that changed into matrix type, as follows:

$$\phi = \begin{Bmatrix} \phi_1 \\ \vdots \\ \vdots \\ \phi_r \end{Bmatrix}, \eta = \begin{Bmatrix} \eta_1 \\ \vdots \\ \vdots \\ \eta_r \end{Bmatrix}, \text{ then}$$

$$y(x,t) = \phi^T\eta = \eta^T\phi \tag{10}$$

Eq. (5) is substituted into Eq. (2), the following conclusion is reached:

$$EI\phi''''^T\eta + c_sI\phi''''^T\dot{\eta} + c_a\phi^T\dot{\eta} + m\phi^T\ddot{\eta} = M(\,g - \phi^T\ddot{\eta} - 2v\phi'^T\dot{\eta} - v^2\phi''^T\eta\,)\delta(x - vt) \tag{11}$$

By multiplying both sides of the Eq. (11) by ϕ,

$$EI\phi\phi''''^T\eta + c_sI\phi\phi''''^T\dot{\eta} + c_a\phi\phi^T\dot{\eta} + m\phi\phi^T\ddot{\eta} = M(\phi\,g - \phi\phi^T\ddot{\eta} - 2v\phi\phi'^T\dot{\eta} - v^2\phi\phi''^T\eta\,)\delta(x - vt) \tag{12}$$

Integrated throughout the 0–L spatial domain, and substitutions based on orthogonality of trigonometric function:

$$\int_0^L (\,EI\phi\phi''''^T\eta + c_sI\phi\phi''''^T\dot{\eta} + c_a\phi\phi^T\dot{\eta} + m\phi\phi^T\ddot{\eta})dx = \int_0^L M(\phi\,g - \phi\phi^T\ddot{\eta} - 2v\phi\phi'^T\dot{\eta} - v^2\phi\phi''^T\eta\,)\delta(x - vt)dx \tag{13}$$

It should be noted that the following Dirac delta function $\delta(x)$ property is used to get the right-hand side of Eq. (13) [21].

$$\int_a^b f(x)\delta(x - X)dx = f(X) \qquad (a < \mathrm{X} < b) \tag{14}$$

For first mode:

$$y(x,t) = \phi_1(x)\eta_1(t) \tag{15}$$

The mass normalised mode shapes are given in Eq. (6)

$$\text{For r=1 } \left(\phi_1(x) = \sqrt{2/mL}\,\sin\,(\pi x/L)\right) \tag{16}$$

Supposing $\phi = \phi_1$, $\eta = \eta_1$, Eq. (13) with rearrange for the equation will be:

$$M_{e1}\frac{d^2\eta(t)}{dt^2} + C_{e1}\frac{d\eta(t)}{dt} + K_{e1}\,\eta(t) = = Mg\sqrt{2/mL}\,sin\,(\pi vt/L) \tag{17}$$

where:

$$M_{e1} = 1 + \frac{2M}{mL}\sin^2\left(\frac{\pi vt}{L}\right)$$
$$C_{e1} = 2\zeta_1\omega_1 + \frac{2M}{mL}\left(\frac{\pi v}{L}\right)\sin\left(2\frac{\pi vt}{L}\right) \tag{18}$$
$$K_{e1} = \omega_1^2 - \frac{2M}{mL}\left(\frac{\pi v}{L}\right)^2\sin^2\left(\frac{\pi vt}{L}\right)$$

$$2\zeta_1\omega_1 = \frac{c_sI\omega_1^2}{EI} + \frac{c_a}{m} \tag{19}$$

$$\omega_1 = \pi^2\sqrt{EI/mL^4} \tag{20}$$

where ζ_1 is the modal mechanical damping ratio and ω_1 is the supported beam's first natural frequency. Thus, the damping ratio ζ_1 contains both viscous air and strain-rate damping effects and can be stated as $\zeta_1 = \zeta_1^a + \zeta_1^s$ where $\zeta_1^a = \frac{c_a}{2m\omega_1}$ and $\zeta_1^s = \frac{c_sI\omega_1}{2EI}$, respectively. The strain-rate damping coefficient seems to be proportional to the stiffness of the structure, but the damping coefficient of viscous air is proportionate to the mass per unit length, as shown in Eq. (19) [9].

2.3. Thin piezoceramic patch

The section discusses a strategy for instances with extremely low oscillation frequency. The slender bridge depicted in Fig. 1 has a piezoceramic patch covering the region $\mathrm{x}_{\mathrm{p}_1} \leq \mathrm{x} \leq \mathrm{x}_{\mathrm{p}_2}$ for generating power from the vibrations caused by the moving mass. is the given section

aims to establish a relationship between the beam's surface strain and the piezoceramic's voltage output. Equation (2) governs the beam's dynamics, and it is assumed that the piezoelectric energy generation and patch have a negligible effect on the beam's dynamics [9].

To derive the equations that govern the electrical behaviour, the supported beam (Fig. 1) with a single layer piezoelectric connected to the external resistance R_l was considered In the case of one-dimensional strain variations, the electric displacement component in the patch's thickness direction is [9].

$$D_3 = \bar{e}_{31} S_1 + \bar{\varepsilon}_{33}^S E_3 \tag{21}$$

Equation (22) depicts the voltage created throughout the load resistance by the piezoelectric patch [9].

$$C_p \frac{dV(t)}{dt} + \frac{V(t)}{R_l} = -\bar{e}_{31} h_{pc} b_p \int_{x_{p_1}}^{x_{p_2}} \frac{\partial^3 y(x,t)}{\partial x^2 \, \partial t} dx \tag{22}$$

where:

$$C_p = \bar{\varepsilon}_{33}^S b_p \left(x_{p_2} - x_{p_1}\right)/h_P \tag{23}$$

$$h_{pc} = \frac{h_P + h}{2} \tag{24}$$

where $C_p, \bar{e}_{31}, \bar{\varepsilon}_{33}^S, b_p, h_P, h_{pc}, h$ represented piezoceramic capacitance, piezoelectric constant, Permittivity constant, the width of piezoceramic, the thickness of piezoceramic, the distance with the neutral axis and beam's thickness respectively.

The solution from Eq. (22) when the beam response in Eq. (5) is substituted:

$$\frac{dV(t)}{dt} + \frac{V(t)}{R_l C_P} = \sum_{r=1}^{\infty} \psi_r \frac{d\eta_r(t)}{dt} \tag{25}$$

where:

$$\psi_r = -\frac{\bar{e}_{31} h_{pc} b_p}{C_p} \int_{x_{p1}}^{x_{p2}} \frac{d^2 \phi_r(x)}{dx^2} dx = \\ = -\frac{\bar{e}_{31} h_{pc} b_p}{C_p} \frac{d\phi_r(x)}{dx}\Big|_{x=x_{p1}}^{x=x_{p2}} \tag{26}$$

For first mode Eq. (25) will be:

$$\frac{dV(t)}{dt} + \frac{V(t)}{R_l C_P} = \psi_1 \frac{d\eta_1(t)}{dt} \tag{27}$$

where:

$$\psi_1 = -\frac{\bar{e}_{31} h_{pc} b_p}{C_p} \int_{x_{p1}}^{x_{p2}} \frac{d^2 \phi_1(x)}{dx^2} dx = \\ = -\frac{\bar{e}_{31} h_{pc} b_p}{C_p} \frac{d\phi_1(x)}{dx}\Big|_{x=x_{p1}}^{x=x_{p2}} \tag{28}$$

$$\frac{d\phi_1(x)}{dx} = \sqrt{2\pi^2/mL^3}\, cos\,(\pi x/L) \tag{29}$$

2.4. Determination of beam deflection and induced voltage of the PZT patch

To obtain the PZT patch voltage, equations (22) and (25) should be solved. The problem was solved numerically. As a result, the system is decomposed into a series of differential first-order equations, and the state variables in the time domain are numerically solved. First vibration mode's state variables are regarded as:

$$x_1(t) = \eta_1(t),\ x_2(t) = \frac{d\eta_1(t)}{dt},\ x_3(t) = V(t) \tag{30}$$

Both modal displacement and velocity are represented by $x_1(t)$ and $x_2(t)$, respectively. At the same time, the induced voltage is $x_3(t)$. Equations (17) and (27) can indeed be described as a number of first-order equations differential:

$$\begin{Bmatrix} \dot{x}_1 \\ \dot{x}_2 \\ \dot{x}_3 \end{Bmatrix} = \begin{Bmatrix} x_2 \\ -\frac{C_{e1} x_2}{M_{e1}} - \frac{K_{e1} x_1}{M_{e1}} + \frac{Mg}{M_{e1}} \sqrt{\frac{2}{mL}}\, sin\, \left(\frac{\pi v t}{L}\right) \\ -\frac{x_3}{R_l C_p} + \psi_1 x_2 \end{Bmatrix} \tag{31}$$

In the study, MATLAB R2017b is utilised to solve the problem of finding beam response and induced voltage of the piezoelectric patch. The key computer software was developed using modern higher-order Eq. (31) and were solved using the Runge-Kutta method in MATLAB. The initial conditions have been set to zero for all equations.

For the first two modes:

$$x_1(t) = \eta_1(t)\ ,\ x_2(t) = \frac{d\eta_1(t)}{dt}\ ,x_3(t) = \eta_2(t)\ , \\ x_4(t) = \frac{d\eta_2(t)}{dt}\ ,x_5(t) = V(t) \tag{32}$$

The power is obtained using root mean square of voltage [9].

$$p_{avg} = \frac{V_{rms}^2}{R_l} \tag{33}$$

3. Experimental rig

Experiments are conducted using a bridge energy harvesting simulator system. This rig is used to simulate bridges of a small size. The rig consists of three main parts: the foundation and the two Substrates. It was constructed from (122 cm x 43 cm x 70 cm) rectangular section iron table and two (13 cm x 13 cm x 10 cm) substrates of a beam supported as shown in Figure 2.

The two substrates were designed to fulfil the requirements for supported conditions. The third part is the sliding stand and the ramp, where the height of the stand and the angle of the plate arc can be changed to control the acceleration of the moving mass. Figure 3 illustrates the data acquisition operations for experimental tests. As the mass moves across the beam, its midpoint displacement is measured using a laser displacement sensor. The sensor's signal is routed straight to a Data Acquisition System (DAQ) and then processed on a computer.

Experimental procedure

The experiment determines the validity and accuracy of the supported beam's analytical and FEM power models. The test rig is depicted in Figure 2. The stainless steel beam utilised in the experiment measures 0.98 m in total length. NI USB-4431 acquisition systems are used in conjunction with the NI-LabVIEW software to monitor -or and analyse the acquired signals. A piezoelectric material is stuck on the beam at the mid-span. The PZT operates as a generator, transforming the mechanical strains generated by the vibrations of the beam to an electrical charge. To compute power, the voltage is passed through a resistor. The resistance is the DAQ impedance for a beam excited by a moving mass function. DAQ is used to determine the voltage across the resistor. The deflection is measured by using a laser displacement sensor. The laser sensor is positioned perpendicular to the midpoint of the beam length and in focus on the beam 4 mm from its edge. The beam surface is cleaned well to ensure that it is free of impurities, especially at both places, the first is where the laser falls to create a highly reflecting surface for the laser and the second is the place where the piezoelectric patch is stuck. The laser sensor measures and transforms the signal to voltage. For this application, the conversion factor is ±5 V (1 mm/V). The damping ratio and the natural frequency of the first vibration mode were also calculated based on the displacement signal, as explained in the next section.

In summary, the moving mass is placed on the ramp to gain acceleration and thus moves at a certain speed according to its position in the ramp. After the moving mass enters the beam, its speed is measured by the four sensors, two of them placed at the beginning and the other at the end of the beam with a distance of 20 cm between every two sensors was kept. From the moment the moving mass enters

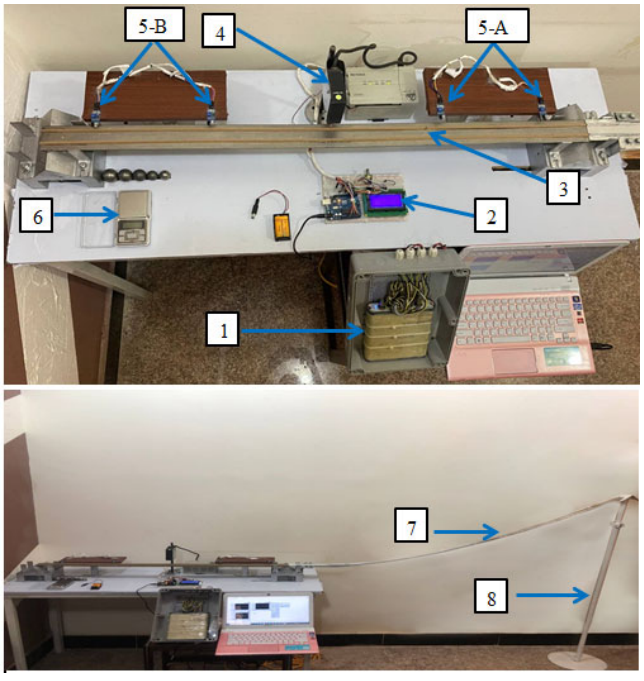

Fig. 2. The designed Rig for experimental assessment, 1) DAQ-4431; 2) Microcontroller; 3) Beam; 4) Laser displacement sensor; 5) IR Sensor (A-At the beginning of beam /B- At the end of beam; 6) Weight Scale; 7) Ramp and; 8) Stand

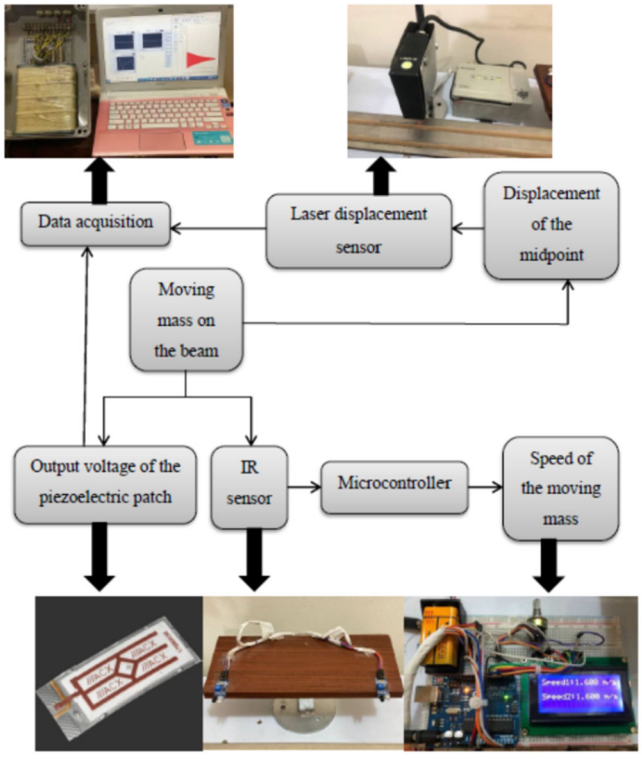

Fig. 3. Diagram for connecting instruments of the experimental rig

the beam until it exits, the deflection of the centre of the beam and the resulting voltage from PZT are measured as shown in Figure 3. Different geometries of piezoelectric produced by the company Mide, the type whose trade name is PPA 1001 was used because it a single layer of PZT material that is well-suited for sensing applications and energy harvesting and its size is compatible with the beam. Moreover, this harvester is sturdy and fairly cheap. The PPA 1001 model is an imorphous sheet made up of a single layer of material PZT 5J piezoelectric layer surrounded by four other layers of structural material in the successions: polymide, copper, PZT 5J, AISI 304 steel and polyester.

4. Results and discussion

4.1. Validation of the proposed model

Using MATLAB R2017b programming, the dynamic deflection of the supported beam under the moving mass is analysed. The results are compared with the approach used for the supported beam used in Cristiano Bilello et al. [5] experimental work. Bilello et al. [6] has developed a scale-model to experimentally examine the response of moving mass-loaded beam. The scale model used in [5] consists of 6061 aluminium beam with L=1053 mm, EI=162.6 Nm^2 and m=1.847 kg/m. The moving mass is 0.5047 kg.

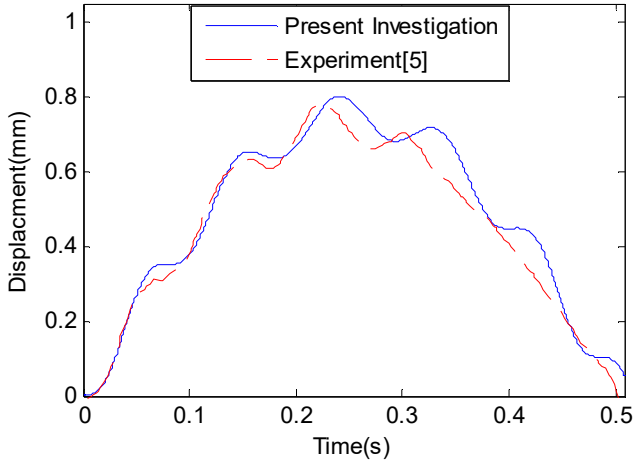

Fig. 4. History of beam deflection at point x=7L/16 for moving mass velocity: 2.1083 m/s

Figure 4 shows the dynamic deflection history of point x=7L/16 for speed 2.1083 m/s. It also shows excellent agreement between the present study and [5] in terms of trend and maximum deflection. The maximum displacement for the experimental [5] and the current investigation is 0.787mm and 0.796 mm, respectively. Thus, the maximum absolute error is 1.12%. The found responses that appear to oscillate following the peak are particularly intriguing. According to the experimental result mentioned in [5], this is most likely generated by out-of-plane oscillations of the moving mass brought on by abnormalities in the rolling surface or guide rails.

4.2. Dynamic deflection results

The results are divided into three parts. Firstly, compare one and first two modes of beam's theoretical displacement, then show the effect of piezoelectric coupling on beam response. Finally, determine the dynamic response of the beam when subjected to a moving mass in various cases. By solving a set of ordinary differential equations in equation (31) using ode45 code in MATLAB and based on the beam specifications which are listed in Table 1, graphs in Figure 5 demonstrate dynamic deflection for the fundamental mode and first two modes of the beam vibration has been obtained. As there was a small discrepancy in the results, it was decided to employ only one mode in subsequent calculations.

Table 1.
The value of parameters employed in the theoretical formulation as a result of the experimental setting

Parameter	Numerical value
L	0.98 m
m	1.17 (kg/m)
I	1.125×10^{-10}m^4
R_l	135 kΩ
b_p	0.0208 m
h_{pc}	0.001575 m
C_p	120.2 nF
L_{pz1}	0.467 m
L_{pz2}	0.513 m
$\bar{\varepsilon}_{33}^{S}$	18.849 nF/m
ζ_1	0.0015
$\bar{e}_{31}$	-17.08 C/m^2

It is well known that beam vibration causes a voltage to be generated in the piezoelectric patch. In general, the piezoelectric patch reacts to the vibration of the beam. A test was conducted to demonstrate the piezoelectric coupling effect's negligibility on the beam deflection. The

piezoelectric patch was mounted to the beam, and then a moving mass moved across it while the piezoelectric was in short-circuit mode and open-circuit mode. As illustrated in Figure 6, the insignificant difference between these two trials confirms the piezoelectric coupling effect's negligibility.

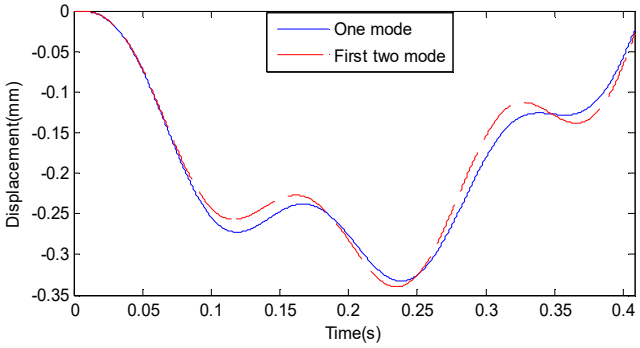

Fig. 5. Comparing the theoretical displacement of the midpoint of the beam under 35.6 g moving mass with 2.4 m/s speed

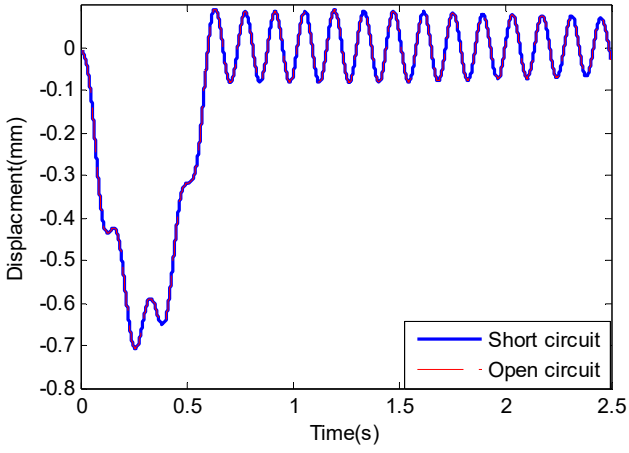

Fig. 6. Comparison of the beam response of piezoelectric patch in the short and open circuit modes for 79.4 gr moving mass with 1.6 m/s speed

The theoretical and experimental dynamic deflection results have been obtained when a constant moving mass traveling at a constant speed crossing from left to right over the beam span. The dynamic analysis of the beam is performed with various moving mass weights and speeds. The midpoint deflection behaviour of a 0.98 m span beam is illustrated in Figure 7 for various moving mass speeds and weights.

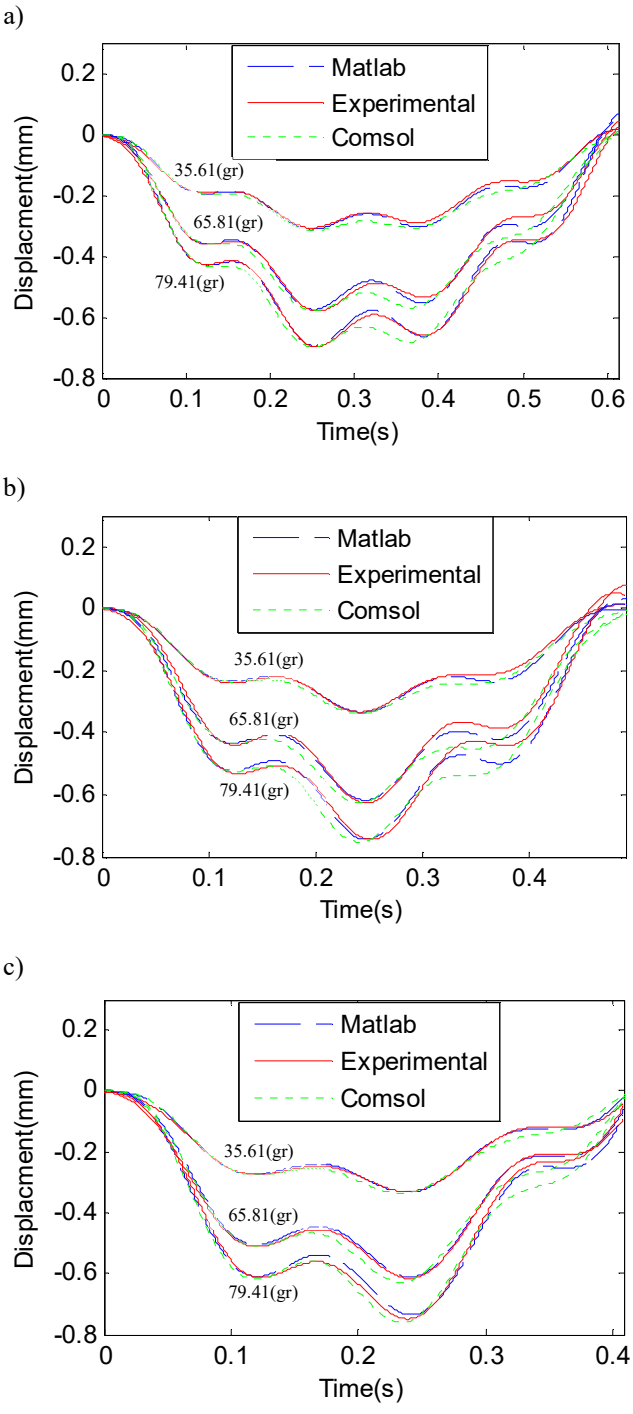

Fig. 7. Comparing the experimental and theoretical displacement of the midpoint of the beam for a) v=1.6 m/s, b) v=2 m/s and c) v=2.4 m/s

The deflection curves for moving masses travelling at speeds of 1.6 m/s, 2 m/s, and 2.4 m/s are presented. As can be seen, the highest deflection occurs at the beam's mid-span point and increases as the moving mass's speed increases. At 1.6 m/s speed, the deflection curve fluctuates more and has a smaller amplitude of variability, whereas at 2.4 m/s, the fluctuation is less, but the amplitude is greater; the reason is due to the resonance frequencies of the coupled dynamic system moving beam-moving mass. Increasing the speed leads to a larger oscillation frequency. Additionally, it is since when speed increases, the energy level of the beam increases.

This variable is altered to adequately examine the weight effect while the remaining values remain constant. As illustrated in Figure 7, when the weight is raised in the following proportions 35.61 gr, 65.81 gr, and 79.41 gr, the maximum displacement gradually increases in proportion with the weight. The behaviour is expected as the global load vector and, subsequently, the displacements, accelerations, and speeds are proportional to the weight according to the linear dynamic system's equations of motion. The displacements of the beam mid-span point are determined using a theoretical approach to mass movement that is generally consistent with those observed experimentally.

As seen from Figure 7, the dynamic deflection caused by a moving mass can be substantially greater than that caused by stationary mass, as the calculated deflection is the result of two components: static and dynamic deflection caused by moving mass.

The maximum displacement of a traversing moving mass does not necessarily occur when the moving mass is at the beam's mid-span region. This phenomenon is caused by both the traversing load's velocity and the reflected waves from the beam's boundary. Figure 7a shows that the maximum deflection occurs when the moving mass travels a distance of 0.415 m from the length of the beam, specifically at the time 0.254 s. That is, we have obtained the maximum deflection of the mid-span of the beam before the mass reaches the middle of the beam.

In Figure 7, small discrepancies are observed between MATLAB and COMSOL results (particularly in the time range [0.3-0.4]) for all three plots because in MATLAB, a one-dimensional piezoelectric model was used. It was solved by ODE45, in contrast to the modelling by COMSOL, where a three-dimensional form of the linear piezoelectric constitutive equations was taken. In addition, a convergence study was performed in COMSOL to determine the appropriate finite element mesh to be used in the structural analysis of the energy harvesting model. Meshes were developed, and with decreasing in element size, it was noticed that the fundamental natural frequency stabilises at optimised square element size equal to "2.8" mm and a number of elements equal to 12772. Therefore, COMSOL results show little variance compared to MATLAB results.

4.3. Piezoelectric energy harvesting results

Next to be obtained and compared are the piezoelectric voltages and power. Figures 8, 9 and 10 display the experimental and theoretical open circuit voltage signals results with time, based on the piezoelectric patch specifications which listed in Table 1. The results reveal that increasing the mass in the following proportions 35.61 gr, 65.81 gr, and 79.41 gr increases the piezoelectric power and voltage at a constant mass speed.

Additionally, when the mass value remains constant, the output of the piezoelectric generator is enhanced by increasing the speed of the moving mass. This is mostly due to the fact that raising the weight of the travelling mass and speed values will increase the beam midpoint deflection and strain. Also, three different moving mass speeds ranging from 1.6 to 2.4 m/s with an interval of 0.4 m/s are adopted for each mass in this study.

It is to be noted that excitation frequency rises as the speed of the moving mass increases, yet the fundamental frequency of the beam remains constant. In Figures 8, 9 and 10 all findings are presented for the period during which the mass is on the beam, i.e., from the time the moving mass comes on the beam until it entirely exits.

The reason why the voltage curve fluctuates more and has a lower amplitude of variability at 1.6 m/s speed compared to 2.4 m/s is because of the resonance frequencies of the coupled dynamic system moving beam-moving mass. A higher oscillation frequency results from increased speed. Additionally, this is because when speed rises, the energy level of the beam rises, which increases the voltage and therefore increases amount of energy harvested.

Table 2 compares the average harvested power obtained experimentally and theoretically from Figures 8, 9, and 10, demonstrating the impacts of increasing the speed and moving mass. Thus, one can increase the amount of energy harvested by increasing the mass or speed of the moving mass. The power shown in Table 2 is calculated using the root mean square of the voltage in accordance with Eq (33).

The Table also shows an acceptable percentage of error when comparing experimental and theoretical results. However, the percentage of error is often lower when comparing COMSEL results with experimental ones, and

that is because the accuracy of the COMSEL for the reasons that were previously explained. For example, for 65.81 gr moving mass with speed 2m/s, the percentage of error in MATLAB is 4.61%, while in COMSOL is 2.28%.

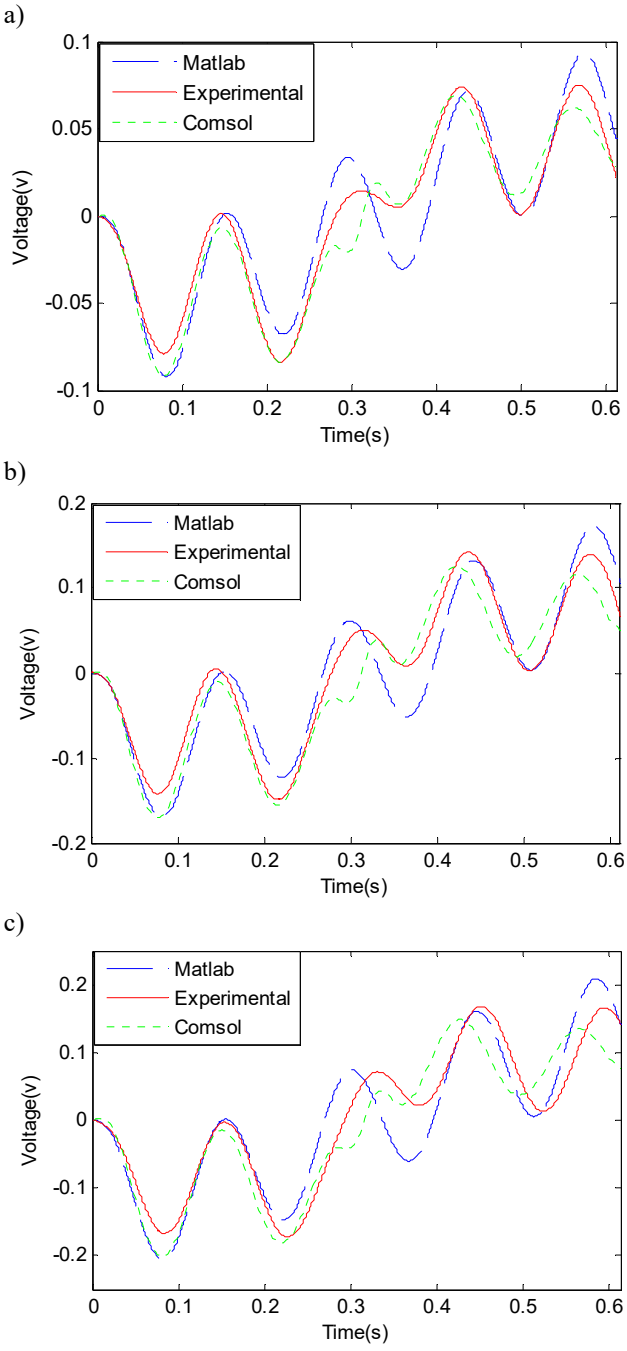

Fig. 8. Experimental and theoretical comparisons of induced open circuit voltage with 1.6m/s for a) 35.61 gr , b) 65.81 gr and c) 79.41 gr

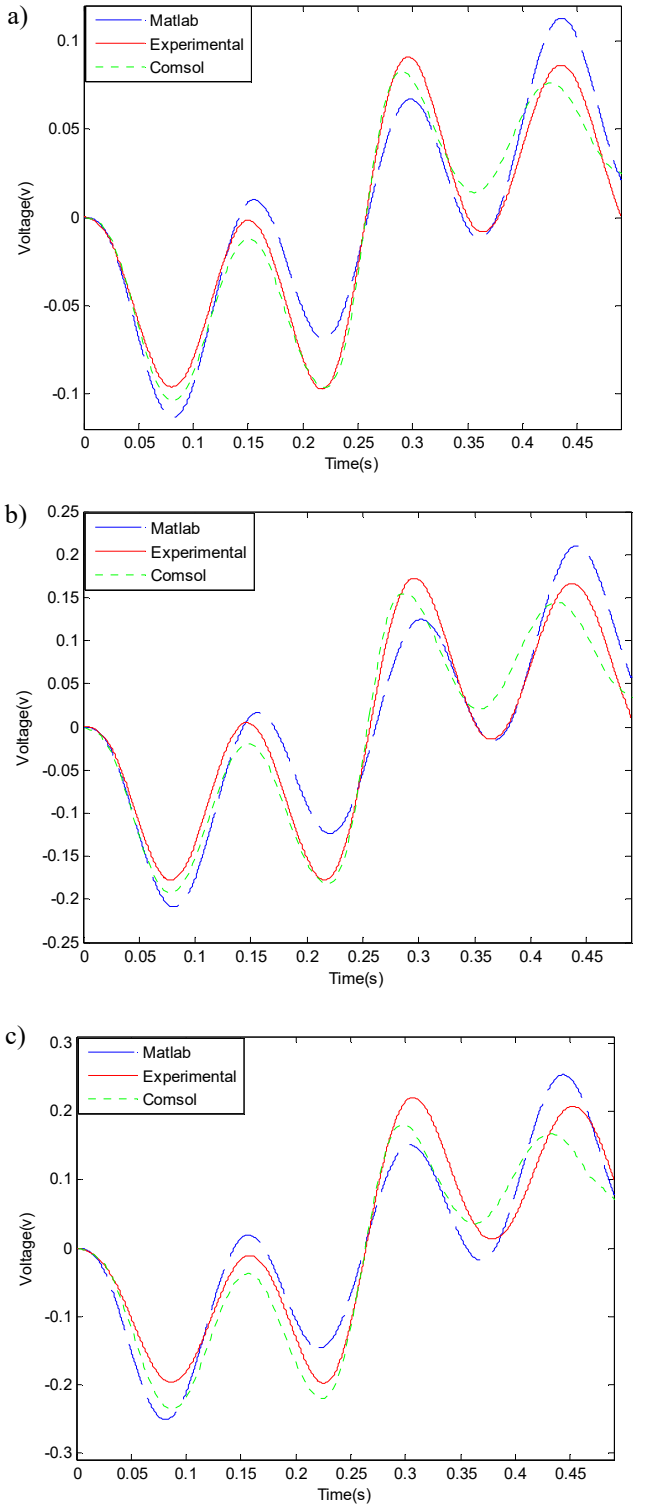

Fig. 9 Experimental and theoretical comparisons of induced open circuit voltage with 2 m/s for: a) 35.61 gr, b) 65.81 gr and c) 79.41 gr

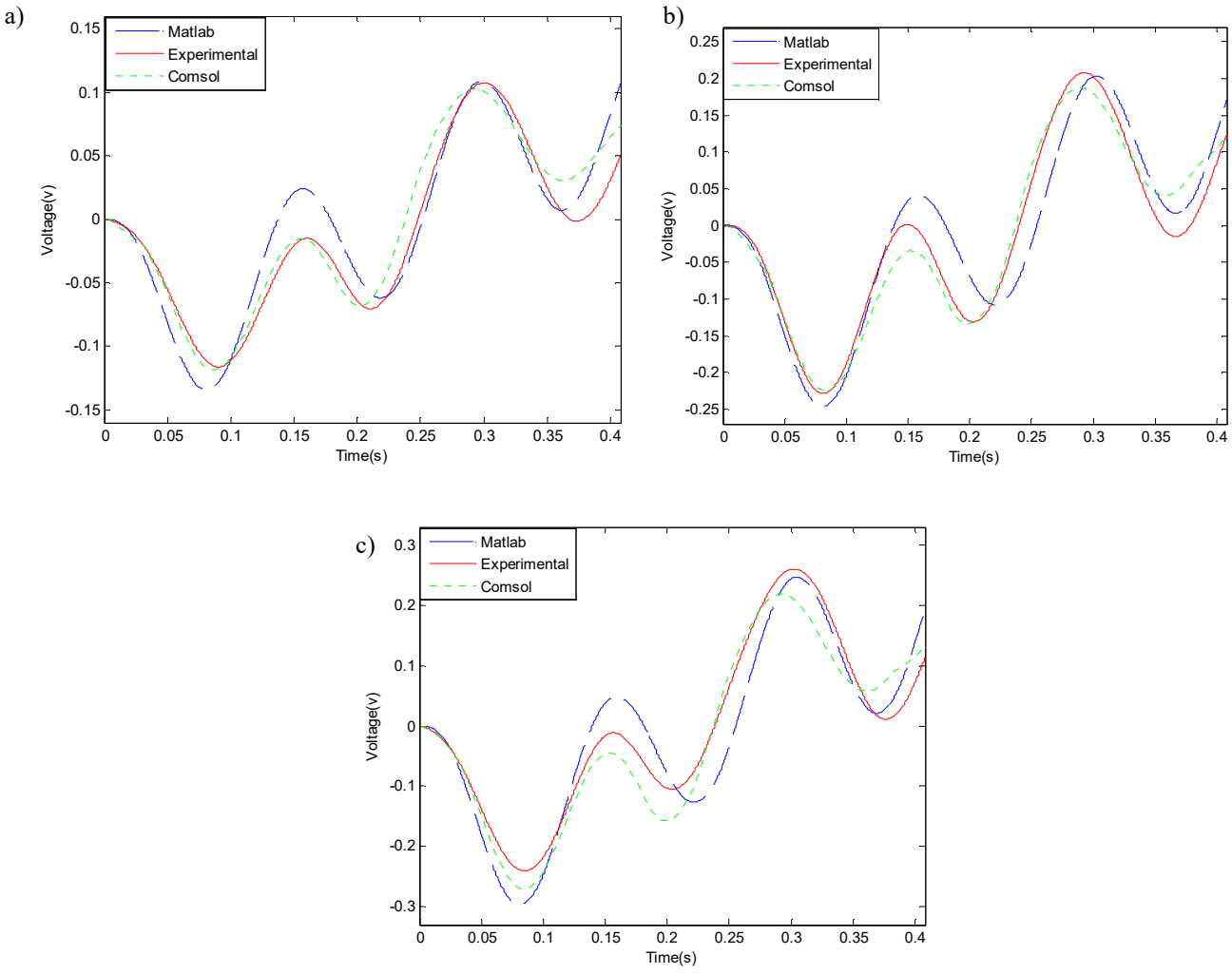

Fig. 10. Experimental and theoretical comparisons of induced open circuit voltage with 2.4 m/s for: a) 35.61 gr, b) 65.81 gr and c) 79.41 gr

Table 2.
Average harvested power value derived from the data supplied in Figures 8, 9 and 10.

Mass, gr	Speed, m/s	Experiment, µW	Matlab, µW	Error, %	Comsol, µW	Error, %
35.61	1.6	0.0156	0.0173	11.025	0.0165	5.38
65.81		0.0532	0.0589	10.833	0.0562	5.656
79.41		0.0759	0.0854	12.608	0.0798	5.174
35.61	2	0.0250	0.0265	5.8841	0.0256	2.6108
65.81		0.0869	0.0909	4.6191	0.0889	2.2832
79.41		0.1305	0.1327	1.7051	0.1331	1.9954
35.61	2.4	0.0296	0.0325	10.082	0.0313	6.0566
65.81		0.1051	0.1093	3.99	0.1083	3.1
79.41		0.1434	0.1583	10.386	0.1537	7.135

Table 3.
Values of fundamental natural frequency with damping ratio

Mass, gr	Speed, m/s	Fundamental natural frequency, Hz			Damping ratio, %
		Experimental	Analytical	COMSOL	
35.61	2.4	7.204	7.261	7.264	0.1547
65.81		7.205			0.1426
79.41		7.209			0.2027

4.4. Effect of the damping ratio

In this part, the state of the simply supported beam is studied after the exciting force acting on it is removed as seen in Figure 11. The damping ratio ζ_1 for the first modevibration was calculated from the experimental results of the displacement-time diagram by the method of logarithmic decrement.

Table 3 shows the fundamental natural frequency, which calculated analytically, numerically and experimentally. Three moving masses with the speed of 2.4 m/s are used each time, the fundamental frequency and damping ratio are measured. The result determined using theoretical approaches are generally consistent with those observed experimentally. The vertical dotted lines in Figure 11 denote the point at which the moving mass exits the beam. After this point, the beam remains vibrating at its natural frequency for period of time.

4.5. Optimisation of variables

This section examines numerous variables parametrically in order to identify how they affect the power output and to optimize the PZT's possible output power coupled to a beam. The parametric investigation will be based on the PZT and beam system described previously.

The investigation will look at the length of the PZT and the resistive load, as well as the length, width and thickness of the beam, will be evaluated and optimised. Finally, the generated power will be estimated using those optimal values. All results were calculated theoretically using an analytical model solved by MATLAB programme.

Load resistance

The output power for various resistive load (R) values may be observed in Figure 12.

Three different moving mass speeds 1.6 m/s, 2 m/s and 2.4 m/s are adopted for each of mass in this study and resistive load ranging 0:30:10000 KΩ where the power output is calculated at each electrical load resistance.

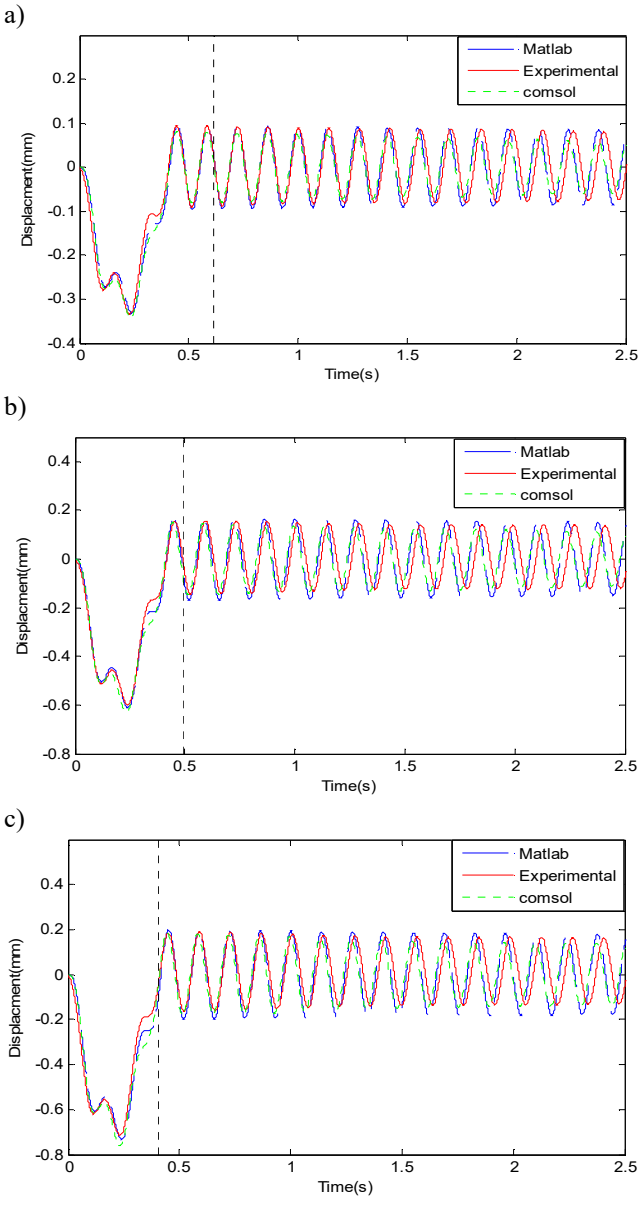

Fig. 11. Time response of the beam at location L/2 and moving mass speed, v= 2.4 m/s for: a) M = 35.61 gr, b) M = 65.81 gr and c) M = 79.41 gr

a)

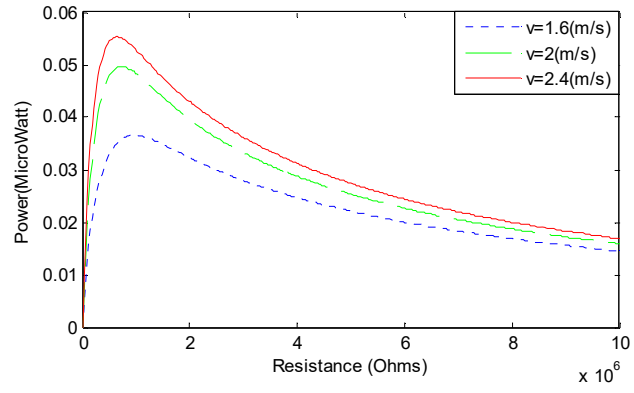

b)

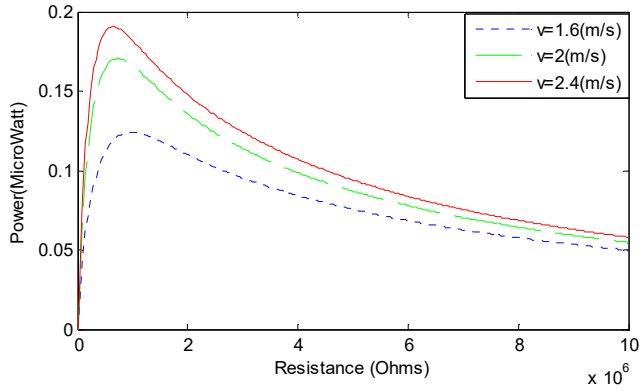

c)

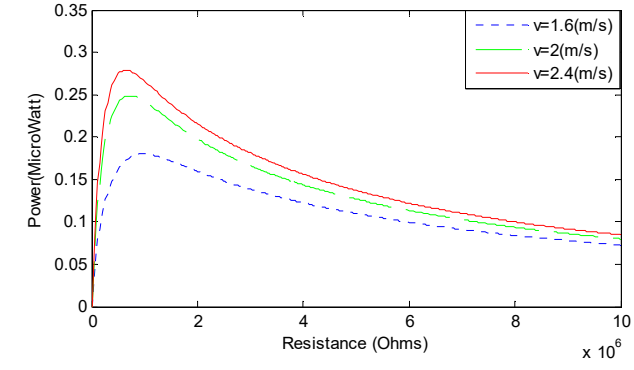

Fig. 12. Harvested power in theory at varying load resistances (R): a) M = 35.61 gr, b) M = 65.81 gr and c) M = 79.41 gr

The optimum resistive load that maximises harvested power can be determined from the Figure 12, for example, with M = 79.41 gr and v = 2.4 m/s, the optimum power is 0.2788 μW at R = 0.63 MΩ. As illustrated in Figure 12, as the moving mass speed increases, the optimal resistive load (R_{OPT}) decreases. Additionally, as the moving mass increases, the harvested power increases**.**

PZT length

The PZT length L_P is the next variable that is optimized. A study is conducted to determine the best length for generating the maximum power. The PZT will begin with a length, L_P, of 0.01 m and will be raised by 0.01 m until it completely fills the beam's length. The length of the PZT is plotted against the output power in Figure 13.

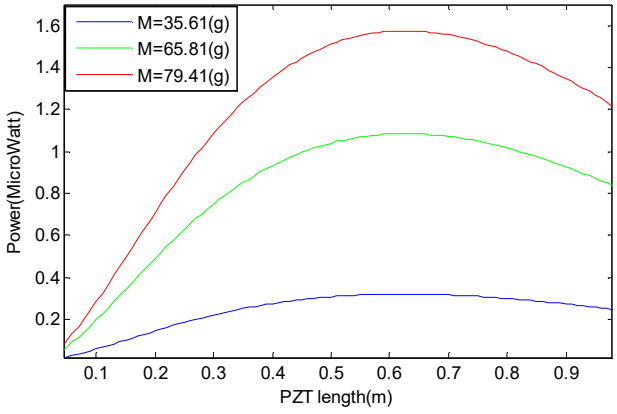

Fig. 13. Output power as a function of the PZT length for moving mass speed 1.6 m/s

In the case of PZT length,larger is not always better. Maximum power is generated at an optimum length of L_P = 0.63 m, or approximately When the piezoelectric patch covers more than half of the beam length. By increasing the PZT surface area thirteen folds, from 0.046 m to 0.63 m, the power output is increased sixteen folds. A trade-off must be made between an increase in the amount of prospective power produced and an increase in the cost of the PZT. Table 4 shows that capacitance increases when increases L_P.

Table 4.
Capacitance and power as function of the PZT length

L_p, m	C_p, nF	Power, μW		
		35.61, gr	65.81, gr	79.41, gr
0.04	105	0.0137	0.0464	0.0673
0.1	261	0.0577	0.1956	0.2832
0.3	784	0.2207	0.7483	1.0848
0.63	1650	0.319	1.0844	1.5746
0.9	2350	0.2722	0.9266	1.3466
0.98	2560	0.246	0.8377	1.2175

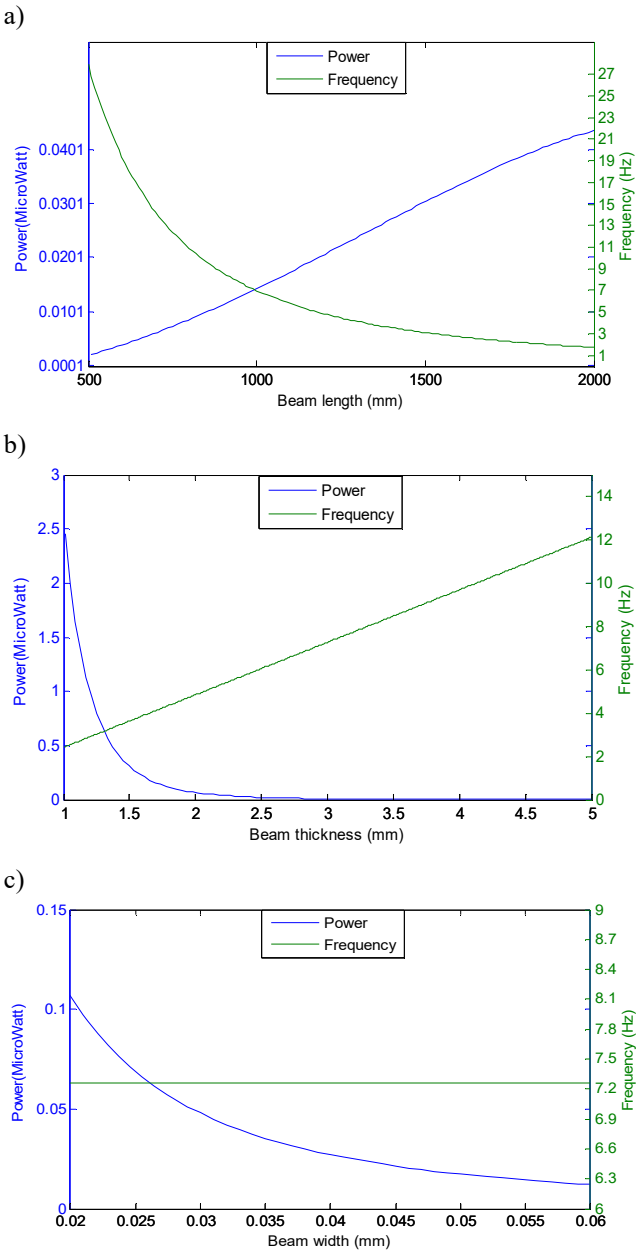

Fig. 14. Resonance frequency and output power as a function of the beam's dimensions a) beam length, b) beam thickness, c) beam width; for moving mass 35.61 gr and move at 1.6 m/s

After a given length of PZT is utilized, it begins to impact the overall parameters of the beam system, affecting the natural frequencies, effective cross-section, and Young's modulus. This will have a detrimental effect, reducing strain affecting the piezoelectric patch, beam deflections, and overall power output.

Dimensions of beam

This study demonstrated how the length, thickness, and width of the simply supported beam affect the resonant frequencies of the beam structure and piezoelectric energy harvesting. As illustrated in Figure 14a, when the thickness and width of the supported beam are fixed, the resonance frequency decreases as the length of the simply supported beam increases.

Moreover, it may compromise the beam's mechanical integrity by going to cause fractures as a result of the increased larger deflections and mass. Also, longer beam increases the amount of energy produced; increasing the length of the beam has an effect on the resonant frequency and the excitation frequency, but its effect on the natural frequency is greater, and therefore, there will be a convergence between the two frequencies, which makes the harvester produce higher energy whenever it vibrates at a frequency close to the resonant frequency. In addition, increasing the beam length leads to an increase in the maximum deflection.

The beam thickness significantly affects the frequency of the simply supported beam. Figure 14b indicates that the frequency is directly proportional to the beam thickness. As the thickness increases, so does the stiffness, which increases the frequency; also the increase led to a decrease of the power produced first because the strain on the piezoelectric will decrease, and secondly, the resonance frequency increases and the excitation frequency is constant.

A wider beam reduces output power, as illustrated in Figure 14c, due to the increased area and mass of the beam but at the same time, that led to reducing the strain; however, the resonance frequency is still constant as long as the structure is a simply supported beam.

5. Conclusions

An electromechanical analytical model for predicting power generation from PZT by an externally excited force represented by a moving mass on supported beam structures has been developed and tested. Several design parameters that affect energy harvesting are being studied in terms of (resistive load, PZT length, as well as the length, thickness, and width of the beam).

The theoretical approach allows the simulation of the behaviour of these harvesters and can provide useful information regarding mechanical aspects. The simulations lead to important applications in the design of these devices and the optimisation of their functional behaviour.

The results are mainly obtained using the analysis method by solving the PDE obtained numerically by MATLAB and then compared to the FEM (numeric method) using COMSOL. The results found by the experiment give good agreement when compared with numerical results.

Some of the conclusions reached through the results of the research are as follows:

1. Analytical and finite element electromechanical models have been developed to forecast energy production from a vibrating of supported beam.
2. The analytical model estimates the properties of piezoelectric elements using the Euler-Bernoulli method. The models accurately anticipate the displacement, voltage, and energy generated by an excited beam by a moving mass. The results of these two models show an agreement with experimental measurements carried out.
3. The maximum dynamic deflection occurs in the half length of the beam regardless of the moving mass's weight or speed, which results in the highest power output when the piezoelectric is positioned in the beam half-length too.
4. The dynamic deflection, piezoelectric voltage, and power all increase as the speed and magnitude of the moving mass increase.
5. Similarly, a parametric analysis was conducted with varying load resistance. It was discovered that the amount of energy harvested changes with the resistance of the energy harvesting circuit. The harvesting power vs load resistance curve begins at zero, increases to a maximum value, and remains almost constant as the resistance increases. For example, the results indicate that the optimum power is 0.2788 μW at a resistance load of 0.63 MΩ for a moving load of M = 79.41 gr at a speed of = 2.4 m/s.
6. By optimising specific variables in the analytical model of the beam, the power generated by the piezoelectric should indeed be increased. The optimal location of the piezoelectric was determined to be adjacent to the mid-span of the beam. The length of the piezoelectric was optimised to be 0.63 m. When the length of the beam increases, the resonant frequency decreases and at the same time, the harvested energy increases. However, increasing the beam thickness has the opposite effect, whereas the beam width value raised does not affect the resonant frequency, but it decreases energy harvesting. To maximize the power output of the piezoelectric harvester, the supported beam should be designed longer, thinner, and narrower, provided that it cannot be fractured.

References

[1] M.A. Ilyas, Piezoelectric Energy Harvesting, Momentum Press, New York, 2018.

[2] E. Blokhina, A. El Aroudi, E. Alarcon, D. Galayko, Nonlinearity in Energy Harvesting Systems Micro and Nanoscale Applications, Springer, Cham, 2016. DOI: https://doi.org/10.1007/978-3-319-20355-3

[3] M.A. Foda, Z. Abduljabbar, A Dynamic Green Function Formulation for the Response of a Beam Structure to a Moving Mass, Journal of Sound and Vibration 210/3 (1998) 295-306. DOI: https://doi.org/10.1006/jsvi.1997.1334

[4] L. Fryba, Vibration of Solids and Structures Under Moving Load, Thomas Telford, London, 1999.

[5] C. Bilello, L.A. Bergman, D. Kuchma, Experimental Investigation of a Small-Scale Bridge Model under a Moving Mass, Journal of Structural Engineering 130/5 (2004) 799-804. DOI: https://doi.org/10.1061/(asce)0733-9445(2004)130:5(799)

[6] S.H. Bakhy, M. Al-Waily, M.A. Al-Shammari, Analytical and numerical investigation of the free vibration of functionally graded materials sandwich beams, Archives of Materials Science and Engineering 110/2 (2021) 72-85. DOI: https://doi.org/10.5604/01.3001.0015.4314

[7] E. Abdeddine, A. Majid, Z. Beidouri, K. Zarbane, Experimental investigation for non-linear vibrations of free supported and cantilever FFF rectangular plates, Archives of Materials Science and Engineering 116/2 (2022) 49-56. DOI: https://doi.org/10.5604/01.3001.0016.1189

[8] S.F. Ali, M.I. Friswell, S. Adhikari, Analysis of Energy Harvesters for Highway Bridges, Journal of Intelligent Material Systems and Structures 22/16 (2011) 1929-1938. DOI: https://doi.org/10.1177/1045389X11417650

[9] A. Erturk, D.J. Inman, Piezoelectric Energy Harvesting, John Wiley & Sons, New York, 2011.

[10] Y. Zhang, S.C.S. Cai, L. Deng, Piezoelectric-based Energy Harvesting in Bridge Systems, Journal of Intelligent Material Systems and Structures 25/12 (2014) 1414-1428. DOI: https://doi.org/10.1177/1045389X13507354

[11] S.S. Murugan, P. Vijayakumar, Identification of ultrasonic frequency for water mist generation using piezoelectric transducer, Archives of Materials Science and Engineering 83/2 (2017) 74-78. DOI: https://doi.org/10.5604/01.3001.0009.9170

[12] K. Bendine, M. Hamdaoui, B.F. Boukhoulda, Piezoelectric Energy Harvesting from a Bridge Subjected to Time-Dependent Moving Loads Using Finite Elements, Arabian Journal for Science and Engineering 44/6 (2019) 5743-5763. DOI: https://doi.org/10.1007/s13369-019-03721-0
[13] Z.-X. Yang, X.-T. He, D.-D. Peng, J.-Y. Sun, Free Damping Vibration of Piezoelectric Cantilever Beams: A Biparametric Perturbation Solution and Its Experimental Verification, Applied Sciences 10/1 (2020) 215. DOI: https://doi.org/10.3390/app10010215
[14] J.X. Wang, J.C. Li, W. Bin Su, X. Zhao, C.M. Wang, A multi-folded-beam piezoelectric energy harvester for wideband energy harvesting under ultra-low harmonic acceleration, Energy Reports 8 (2022) 6521-6529. DOI: https://doi.org/10.1016/j.egyr.2022.04.077
[15] C. Xiong, N. Wu, Y. He, Y. Cai, X. Zeng, P. Jin, M. Lai, Nonlinear Energy Harvesting by Piezoelectric Bionic 'M' Shape Generating Beam Featured in Reducing Stress Concentration, Micromachines 14/5 (2023) 1007. DOI: https://doi.org/10.3390/mi14051007
[16] M. Dehestani, M. Mofid, A. Vafai, Investigation of Critical Influential Speed for Moving Mass Problems on Beams, Applied Mathematical Modelling 33/10 (2009) 3885-3895. DOI: https://doi.org/10.1016/j.apm.2009.01.003
[17] H. Han, X. Qiu, Z. Xu, R. Bai, Vibration Analysis of the Beam Structure under the Moving Mass, Vibroengineering Procedia 5 (2015) 446-451.
[18] D.R. Parhi, A.K. Behcra, Dynamic Deflection of a Cracked Beam with Moving Mass, Proceedings of the Institution of Mechanical Engineers, Part C: Journal of Mechanical Engineering Science 211/1 (1997) 77-87. DOI: https://doi.org/10.1243/0954406971521674
[19] L. Meirovitch, Elements of Vibration Analysis, Second Edition, McGraw-Hill, NewYork, 1986.
[20] M.J. Jweeg, D.A. Alazawi, Q.H. Jebur, M. Al-Waily, N.J. Yasin, Hyperelastic modelling of rubber with multi-walled carbon nanotubes subjected to tensile loading, Archives of Materials Science and Engineering 114/2 (2022) 69-85. DOI: https://doi.org/10.5604/01.3001.0016.0027
[21] V. Kahya, Dynamic analysis of pre-stressed elastic beams under moving mass using different beam models, Challenge Journal of Structural Mechanics 1/3 (2015) 106-116. DOI: https://doi.org/10.20528/cjsmec.2015.06.018